ADVANCED FUNCTIONAL MATERIALS
www.afm-journal.de

# Ternary Thermosensitive Hydrogel-Encapsulated Macrolactam Heneicosapeptide Eliminates Epidermal Multidrug-Resistant Bi-Microbial Colonization

*Ping Zeng, Pengfei Zhang, Lanhua Yi, Honglan Wang, Wei Gao, Liang Yao, Lei Zhang, Pu Chen, Kwok-Yin Wong, Sheng Chen, Sharon Shui Yee Leung,* and Kin-Fai Chan**

**Superbug epidemic has rendered antibiotic therapeutics increasingly ineffective. Worse still, there are few applicable medication regimens for polymicrobial infections caused by two or more multidrug-resistant bacteria. Herein, a panel of antibacterial cyclic peptides are designed and synthesized and the lead compound cyclo-zp80r shows favorable activities against a broad spectrum of bacteria. Encouragingly, it exhibited a strong bactericidal effect against two important epidermic species *Pseudomonas aeruginosa* and *Staphylococcus aureus* for both single- and co-infections. The peptide cyclo-zp80r is proposed to destroy the membrane structures of both Gram-negative and Gram-positive bacteria, inducing a variety of physiological disorders. To better adapt to topical administration of this novel antibacterial agent, a hydrogel formulation consisting of poloxamer 407, poloxamer 188, and hyaluronic acid is optimized. This ternary hydrogel system is able to form in situ gel at skin temperature. Encapsulated peptide molecules are released steadily in both human skin ex vivo model and mouse wound in vivo model to treat bi-microbial infection. This work systematically investigates the design, synthesis, antibacterial mechanism of a novel cyclic peptide, and its drug delivery strategy for topical wound infection, offering a promising therapeutics to treat multidrug-resistant polymicrobial wound infections.**

## 1. Introduction

Open wounds can be a breeding ground for bacterial reproduction, causing pathogenic infections, bacteremia, and even death for severe cases.[1] In this post-antibiotic era, patients and physicians urgently call for new and more effective antibacterials.[2] According to the World Health Organization, only 13 novel antibiotics are currently in phase III clinical trials. If no effective treatment strategies become available, the death toll caused by multidrug-resistant (MDR) bacterial infections may reach 10 million per year globally by 2050.[3]

Among common epidermic microbes, *Pseudomonas aeruginosa* (*PA*) and *Staphylococcus aureus* (*SA*) are extremely concerned and are listed as two out of the six notorious ESKAPE bacteria.[4] Co-existence of Gram-negative *PA* and Gram-positive *SA* in the same micro-environment further exacerbates the difficulty of rational treatments.[5] From the perspective of

P. Zeng, P. Zhang, H. Wang, S. S. Y. Leung
School of Pharmacy
Faculty of Medicine
The Chinese University of Hong Kong
Shatin, Hong Kong 999077, China
E-mail: sharon.leung@cuhk.edu.hk

P. Zeng, K.-Y. Wong, K.-F. Chan
State Key Laboratory of Chemical Biology and Drug Discovery and Department of Applied Biology and Chemical Technology
The Hong Kong Polytechnic University
Hung Hom, Kowloon, Hong Kong 999077, China
E-mail: kf.chan@polyu.edu.hk

The ORCID identification number(s) for the author(s) of this article can be found under https://doi.org/10.1002/adfm.202420652



**DOI: 10.1002/adfm.202420652**

L. Yi
College of Food Science
Southwest University
Chongqing 400715, China

W. Gao
School of Materials Science and Engineering
Shanghai Institute of Technology
Shanghai 201418, China

L. Yao
School of Biotechnology
Jiangsu University of Science and Technology
Zhenjiang, Jiangsu 212003, China

L. Zhang, P. Chen
Department of Chemical Engineering
University of Waterloo
Waterloo, ON N2L 3G1, Canada

S. Chen
Department of Food Science and Nutrition
Faculty of Science
The Hong Kong Polytechnic University
Hung Hom, Kowloon, Hong Kong 999077, China

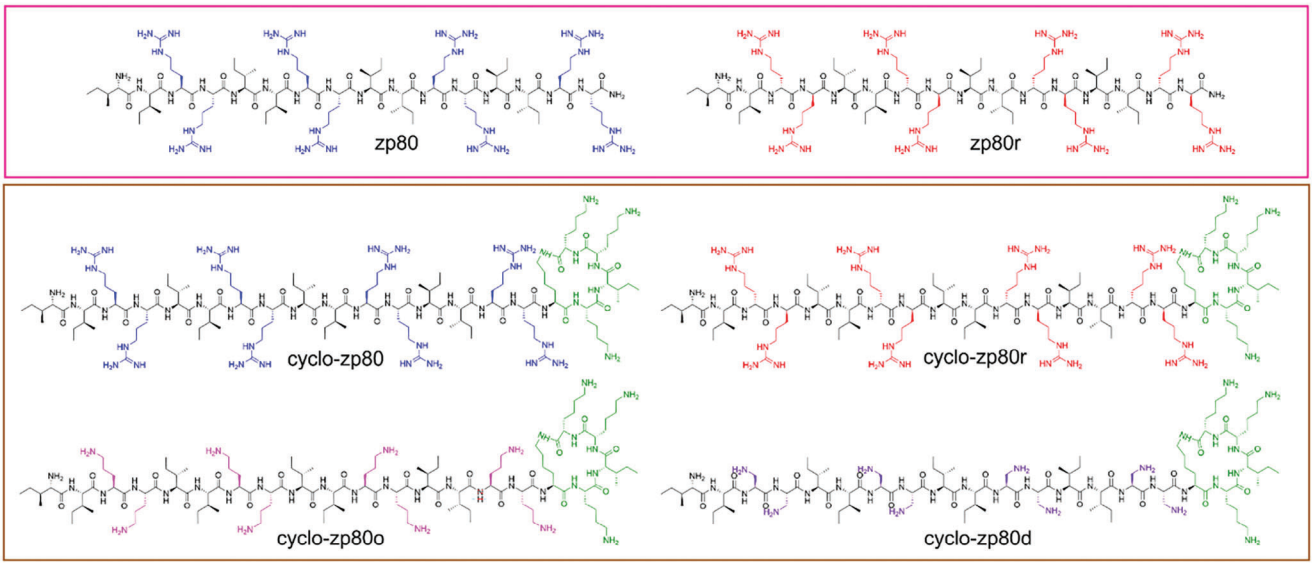


**Figure 1.** Chemical structures of *de novo* designed peptides. Variable positions are highlighted in blue (L-Arg), red (D-Arg), pink (ornithine), purple (2,3-diaminopropionic acid), and green (macrolactam capping), respectively.

broad-spectrum bioactivity, the membrane-targeting antimicrobial peptide (AMP) is a promising class of antibacterial agent.[6] This type of molecule generally possessed amphiphilicity and cationicity, conferring its excellent affinity with the lipid bacterial membrane.[7] Many AMPs were reported to be noncytotoxic to normal cells, but able to kill both Gram-negative and Gram-positive pathogens.[8]

We previously synthesized a $\alpha\alpha\beta\beta$-type ($\alpha$: hydrophobic amino acid; $\beta$: hydrophilic amino acid) linear peptide $(IIRR)_4$-$NH_2$ (**zp80**) with a broad antibacterial spectrum.[9] Unfortunately, subsequent experiments revealed that this peptide showed weak stability in the presence of proteases and high cytotoxicity in vitro, which may severely hamper its potential clinical application. Compared with linear peptides, cyclic AMPs pose higher therapeutic potential as they generally have improved proteolytic stability.[10] Therefore, we modified **zp80** in two directions in the present study. First, we substituted L-Arg to unnatural cationic amino acids like D-Arg (r), ornithine (O) or *S*-2,3-diaminopropionic acid (Dap). Second, we conjugated a macrolactam ring at the *C*-terminal to obtain an optimum balance between the antibacterial activity and toxicity to mammalian cells. These efforts resulted in four head-to-side chain cyclic AMPs. Their antibacterial and hemolytic activities were systematically measured. Then, the lead compound was chosen for further investigation into its possible mode of action.

On-demand release of bioactive molecules is also a challenge.[11] Reasonable design of delivery system will maximize the antibacterial effects.[12] Given that free drug solution may not be effectively retained at the wound site to achieve effective treatment against wound infections, we therefore formulated the designed peptide into a ternary thermosensitive hydrogel comprised of poloxamer 407 (P407), poloxamer 188 (P188) and hyaluronic acid (HA). This in situ hydrogel wound dressing allowed sustained release of the incorporated peptide at the infection site to prolong the therapeutic effect. Its antibacterial efficacy was validated in both *ex vivo* human skin and in vivo mouse wound infection models. Overall, this work reported an original cyclic peptide therapeutic against bi-microbial wound infection associated with *PA* and *SA* with an effective hydrogel delivery system.

## 2. Results and Discussion

### 2.1. Design, Synthesis, and Bioactivity of Engineered Peptides

L-Arg is considered to be a high-risk cleavage site to enzymes like trypsin.[13] Therefore, we first substituted all L-Arg residues in **zp80** with corresponding D-Arg and obtained $(IIrr)_4$-$NH_2$ (**zp80r**). Subsequently, by conjugating a KKIKK macrolactam ring at the *C*-terminal of $(IIRR)_4$, $(IIrr)_4$, $(IIOO)_4$, and $(IIDapDap)_4$ respectively, four cyclic AMPs termed **cyclo-zp80**, **cyclo-zp80r**, **cyclo-zp80o** and **cyclo-zp80d** were engineered. The cyclization was achieved by attaching the $\alpha$-amino of $Lys^{17}$ with the prior residue, followed by linking the side chain amino group with the carboxyl group of $Lys^{21}$ via lactamization, forming head-to-side chain cyclic AMPs (**Figure 1**).

Structurally, they were classified as heneicosapeptides with 16 exocyclic amino acids and 5 ring-formation residues. Crude products were purified by high-performance liquid chromatography (HPLC) and then identified by electrospray-ionization mass spectrometry (MS). Their basic physical properties are listed in **Table 1**. MS and HPLC profiles of individual cyclic peptides are shown in Figures S1–S6 (Supporting Information).

To gain a comprehensive understanding of the antimicrobial spectrum of the designed peptides, we first evaluated their minimum inhibitory concentrations (MICs) against various bacterial species. Tested strains were categorized into four groups: Gram-negative standard, Gram-positive standard, Gram-negative clinical isolates, and Gram-positive clinical isolates. Encouragingly, all engineered peptides shared a similarly broad antibacterial activity. These data indicated that substituting L-Arg to other cationic residues and capping a KKIKK pentapeptide cycle would not

**Table 1.** Physical properties of engineered peptides.

| Peptide | Molecular weight | Retention time [min] | Net charge | Purity |
|---|---|---|---|---|
| **zp80** | 2171.8 | 10.9 | +9 | 99% |
| **zp80r** | 2171.8 | 9.5 | +9 | 95% |
| **cyclo-zp80** | 2780.7 | 8.1 | +12 | 95% |
| **cyclo-zp80r** | 2780.7 | 10.0 | +12 | 95% |
| **cyclo-zp80o** | 2447.3 | 12.0 | +12 | 91% |
| **cyclo-zp80d** | 2222.9 | 11.6 | +12 | 90% |

abolish the potent antibacterial activity of the parent peptide **zp80**. Here, we introduced three approved antibitics as positive controls, including colistin, vancomycin, and meropenem belonging to cyclic peptide, glycopeptide, and carbapenem antibiotics, respectively. Although they are still used clinically, a large number of drug-resistant strains have been reported, challenging their application range.[14]

As illustrated in the heatmap (**Figure 2A**), colistin performed well in killing Gram-negative bacteria, but showed significantly weaker bioactivities against Gram-positive pathogens. On the contrary, vancomycin exhibited favorable bioactivities against Gram-positive bacteria only. In comparison, meropenem demontrated a much broader antibacterial spectrum against both Gram-negative and Gram-positive standard strains. However, it struggled to combat clinical isolates, especially those carbapenem-resistant superbugs (individual MIC values can be found in Table S1, Supporting Information). Average MICs shown in Figure 2B clearly revealed that our designed peptides have outperformed abovementioned three antibiotics from a holistic perspective. In particular, the average MICs of **cyclo-zp80r** to four classes of bacterial strains were all lower than 4 μM.

Next, the toxicity of **cyclo-zp80r** to a human keratinocyte cell line HaCaT and rat red blood cell (RBC) was investigated, respectively. The result showed that **cyclo-zp80r** demonstrated relatively low cytotoxicity to HaCaT with the half inhibition concentration ($IC_{50}$) higher than 64 μM (Figure 2C). Furthermore, compared with the linear counterpart **zp80r**, capping a KKIKK macrolactam ring dramatically led to the hemolytic incapacitation (Figure 2D).

We initially detected the inhibitory capability and killing effect of **cyclo-zp80r** against two selective superbugs *PA* 03 and *SA* 11I4. As mentioned before, *PA* and *SA* are the leading Gram-positive and Gram-negative pathogens, respectively, isolated in wound infections, and their mixed colonization was frequently reported.[15] Growth curves by measuring the dynamic changes of optical density at 600 nm ($OD_{600}$) values suggested that **cyclo-zp80r** at sub-MIC level could partially restrain the cellular proliferation of *PA* 03 and *SA* 11I4 (Figure S7, Supporting Information). In the presence of 16 μM **cyclo-zp80r**, *PA* 03 (Figure 2E) and *SA* 11I4 (Figure 2F) cells could be eradicated within 2 and 4 h, respectively. The downtrend of colony colony-forming unit (CFU) verified that **cyclo-zp80r** killed these pathogens rapidly. Peptide **cyclo-zp80r** exhibited similar killing kinetics compared with two approved peptide-based antibiotics colistin and vancomycin at the same concentrations, 16 μM. Figure 2G shows no visible colonies after 18 h treatment of 2 μM **cyclo-zp80r** for *PA* 03 and 4 μM **cyclo-zp80r** for *SA* 11I4, indicating their respective minimum bactericidal concentrations (MBC).

### 2.2. Physical Properties of the Lead Peptide Cyclo-zp80r

Proteolytic stability has always been a big challenge for peptide drugs.[16] The tolerance of designed AMPs to enzymatic hydrolysis was measured. In the presence of 4 μg $mL^{-1}$ trypsin, the fold change in MIC of **zp80** and **cyclo-zp80** against *PA* 03 (**Figure 3A**) and *SA* 11I4 (Figure 3B) were both 32. These results implied that the macrolactam ring could not stabilize the peptide from enzymatic degradation at high concentrations of trypsin. We speculated that the pentapeptide cycle was too small to creat sufficient steric hindrance and protect the long linear section from trypsin attack. In contrast, the MICs of **zp80r** and **cyclo-zp80r** were maintained throughout the range of trypsin concentration tested, suggesting that the replacement of L-Arg with the D-Arg would enhance proteolytic stability. This may be because trypsin failed to recognize the residues after chiral changes. HPLC chromatogram in Figure 3C further proved that exposing at 2 μg $mL^{-1}$ trypsin for 6 h would not result in hydrolysis of **cyclo-zp80r** molecules (peak area ratio 98.34%). While both the linear and cyclic counterparts showed excellent antibacterial activities, **cyclo-zp80r** was considered a more promising therapeutic candidate because of the significantly lower hemolytic activity, even though the synthetic difficulty and high cost of unnatural D-Arg.

Compared with the trypsin solution, serum is a more complicated environment that contains incomputable enzymes and cellular activity factors.[17] We then monitored the $OD_{600}$ values of bacterial solutions in the absence or presence of **cyclo-zp80r** at different volume ratio of fetal bovine serum (FBS). Figure 3D shows both *PA* 03 and *SA* 11I4 cells were able to proliferate in all tested serum concentrations in the absence of peptide, reaching $OD_{600}$ values >1.5 after 18 h incubation. While in the presence of **cyclo-zp80r** at their respective MICs, *PA* 03 and *SA* 11I4 failed to grow even in 100% serum, demonstrating the excellent stability of **cyclo-zp80r** in extreme serum environments.

Due to the favorable bioactivity and stability, **cyclo-zp80r** was chosen as the lead compound. The obvious structural transformation was detected by circular dichroism (CD) spectroscopy from pure water to an amphiphilic solution (Figure 3E). The predicted helix ratio reduced from 13.4% in water to 3.8% in 50 mM sodium dodecyl sulfonate (SDS), while the antiparallel ratio increased dramatically from 22.1% to 68.8%. This hinted that **cyclo-zp80r** had a flexible chemical structure, which could be induced by amphiphilic interfaces, such as cell membranes. **Cyclo-zp80r** possesses a long linear $(IIrr)_4$ chain and a KKIKK macrolactam tail, whose preferred conformation model is predicted in Figure 3F.

### 2.3. Activity Against Bacterial Persisters and Resistance Development

Nutrient deprivation may lead to starvation-induced antibiotic tolerance. These "hungry" microbes, also termed persisters, normally exhibit decreased sensitivities against traditional antibacterials.[18] Herein, we investigated whether this phenomenon applied to **cyclo-zp80r**. Initially, MICs of colistin and **cyclo-zp80r** to *PA* 03 were 1 and 2 μM, respectively. After 72 h starvation treatment, MIC of colistin increased 8 fold while **cyclo-zp80r** only doubled (**Figure 4A**). Interestingly, Gram-positive

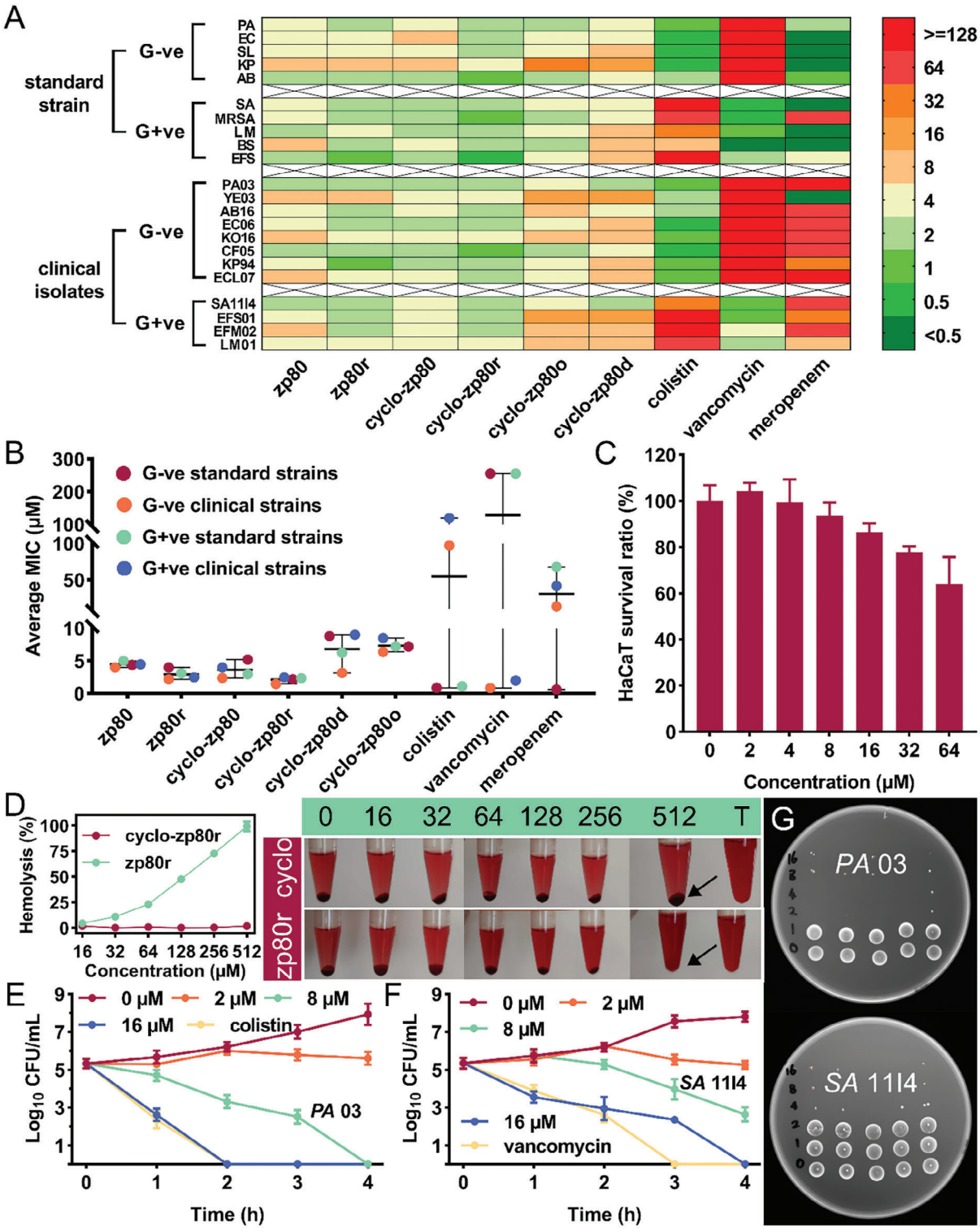


**Figure 2.** A) MIC values of designed peptides and approved antibiotics colistin, vancomycin, and meropenem against various bacterial strains. *PA*, *Pseudomonas aeruginosa* ATCC 15692; *EC*, *Escherichia coli* ATCC 25922; *SL*, *Salmonella typhimurium* PY1; *KP*, *Klebsiella pneumoniae* ATCC 78578; *AB*, *Acinetobacter baumannii* ATCC 19606; *SA*, *Staphylococcus aureus* ATCC 29213; *MRSA*, methicillin-resistant *Staphylococcus aureus* ATCC 1717; *LM*, *Listeria monocytogenes* ATCC 19114; *BS*, *Bacillus subtilis* ATCC 23857; *EFS*, *Enterococcus faecalis* ATCC 29212; *YE*, *Yersinia enterocolitica*; *KO*, *Klebsiella oxytoca*; *CF*, *Citrobacter freundii*; *ECL*, *Enterobacter cloacae*; *EFM*, *Enterococcus faecium*; B) Average MIC values of designed peptides and approved antibiotics; C) Cytotoxicity of **cyclo-zp80r** to HaCaT cells; D) Hemolysis of **zp80r** and **cyclo-zp80r** to rat RBCs. The black arrows highlight hemolytic scenarios in high concentrations of peptides and T indicates 0.1% Triton X-100; The time-killing curves of *PA* 03 E) and *SA* 11I4 F) in the presence of **cyclo-zp80r** or 8 μM of antibiotics colistin/vancomycin; G) MBC of **cyclo-zp80r** to *PA* 03 and *SA* 11I4.

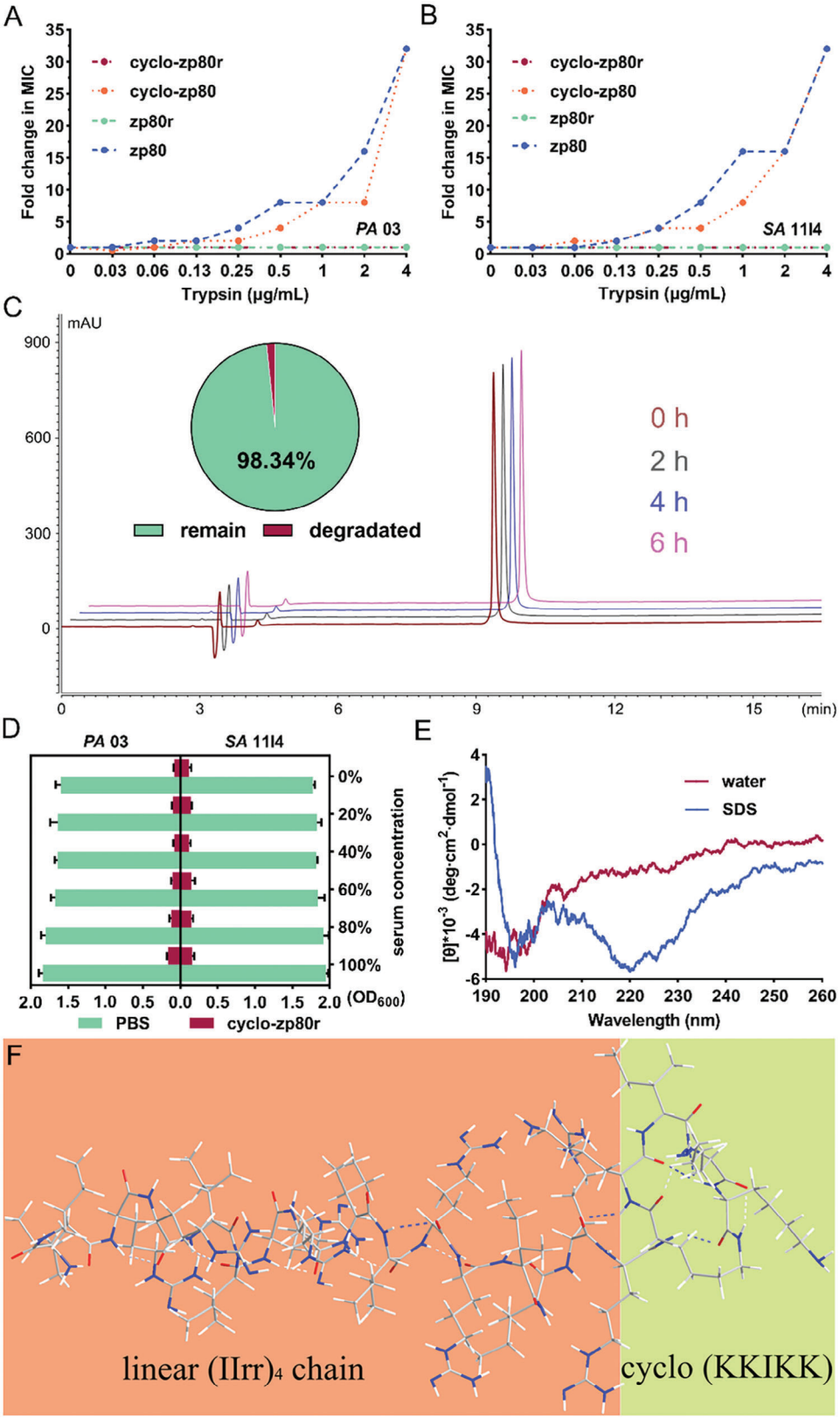


**Figure 3.** MIC fold change to *PA* 03 A) and *SA* 1114 B) of designed peptides in the presence of trypsin; C) HPLC analysis of **cyclo-zp80r** before and after trypsin treatment; D) $OD_{600}$ values of *PA* 03 and *SA* 1114 at different FBS concentration gradients after PBS or **cyclo-zp80r** treatment; E) CD spectroscopy of **cyclo-zp80r** in water and 50 mM SDS solutions; F) predicted preferred conformation model of **cyclo-zp80r**.

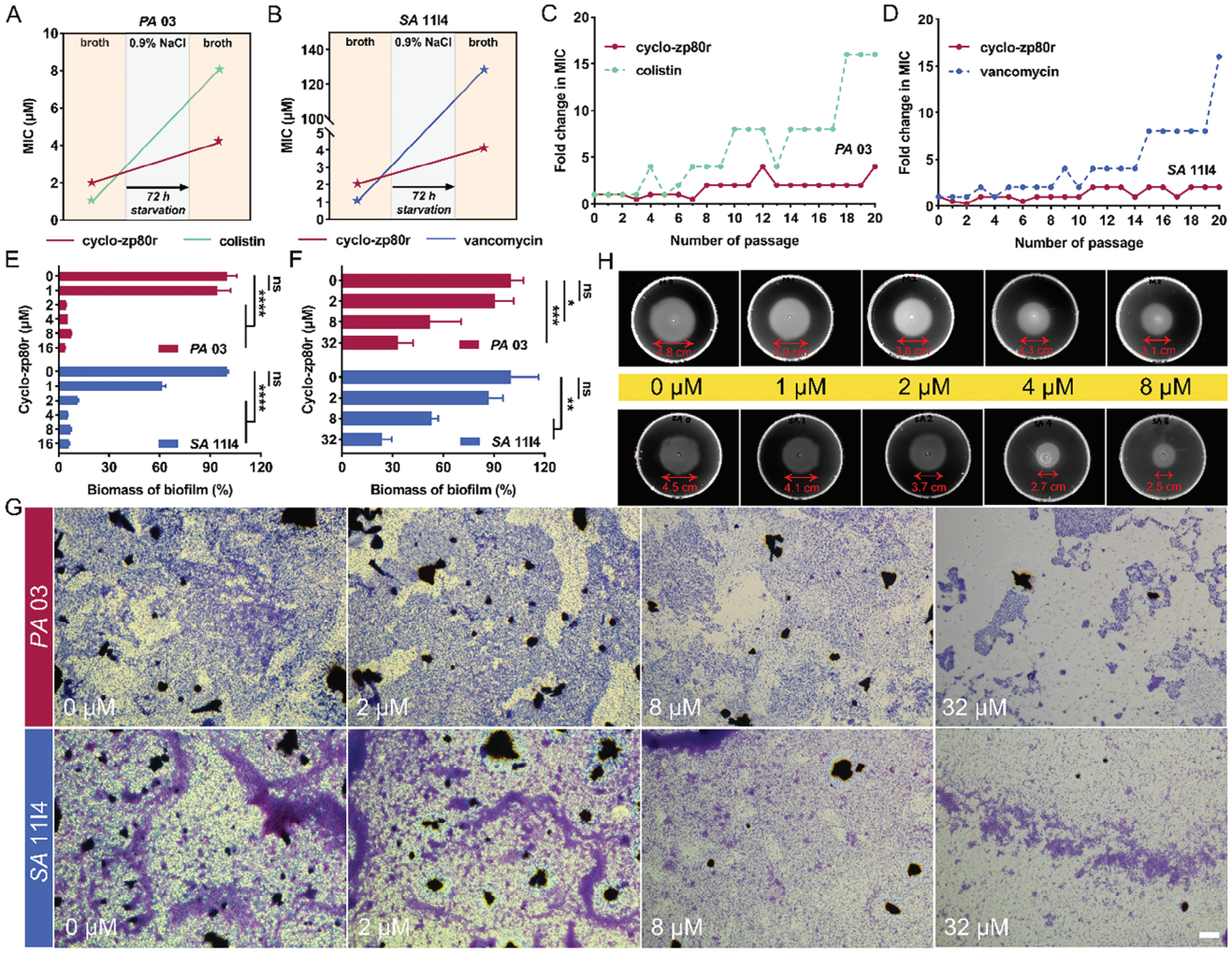


**Figure 4.** MIC change of colistin and **cyclo-zp80r** against *PA* 03 A) and *SA* 11I4 B) before and after 72 h starvation induction; Development of drug resistance of *PA* 03 C) and *SA* 11I4 D); Biofilm formation inhibition E) and preformed biofilm eradication F) of **cyclo-zp80r**; G) Crystal violet staining images of *PA* 03 and *SA* 11I4 biofilm treated with 0, 2, 8 and 32 μM of **cyclo-zp80r**. Scale bar: 100 μm; H) Swarming motility inhibition of **cyclo-zp80r** to *PA* 03 (upper) and *SA* 11I4 (lower).

strain *SA* 11I4 facing starvation induction showed a more significant change (Figure 4B). The MIC of vancomycin soared from 1 μM to 128 μM. In comparison, this value only mildly elevated from 2 to 4 μM for **cyclo-zp80r**.

Frequent exposure to sublethal antibacterial treatment may transform sensitive bacteria to resistant ones.[19] To monitor the development of resistance, we employed sub-MIC screening assay to test drug sensitivities within 20 passages (Figure 4C,D). After continuous treatment, *PA* 03 and *SA* 11I4 gradually showed resistance to colistin and vancomycin. In the final passage, MIC of colistin against *PA* 03 was 4-fold higher than that of **cyclo-zp80r**. Similarly, MIC of vancomycin against *SA* 11I4 was 8-fold higher than that of **cyclo-zp80r**.

Besides planktonic movement, bacterial cells tend to generate extracellular polymeric substance-based biofilm to evade antibiotics in a restricted space.[20] These self-produced compact matrix exacerbated the difficulty of rational treatments since they dramatically reduce the penetration efficiency of many antibacterial drugs.[21] Therefore, antibiofilm activity of **cyclo-zp80r** was measured. In Figure 4E, a concentration of 2 μM **cyclo-zp80r** could effectively inhibited the formation of biofilms to <15% biofilm biomass as the untreated controlled groups for both *PA* 03 and *SA* 11I4. These values were consistent with the MIC observations, suggesting that **cyclo-zp80r** led to rapid bactericidal effect ahead of biofilm formation. Figure 4F shows that **cyclo-zp80r** was also able to eradicate preformed biofilm, but a higher concentration was required. The biofilm elimination effect was also visualized by crystal violet images (Figure 4G). Dense and compact *PA* 03 or *SA* 11I4 biofilm can be observed in the control group. After treatment with 2, 8, and 32 μM of **cyclo-zp80r**, area stained by crystal violet shrank, suggesting that the peptide destroyed the preformed biofilms in a dose-dependent manner.

Swarming motility, a rapid multicellular movement across a solid surface, is an important indicator to evaluate bacterial viability and spread velocity.[22] Many studies have paid close

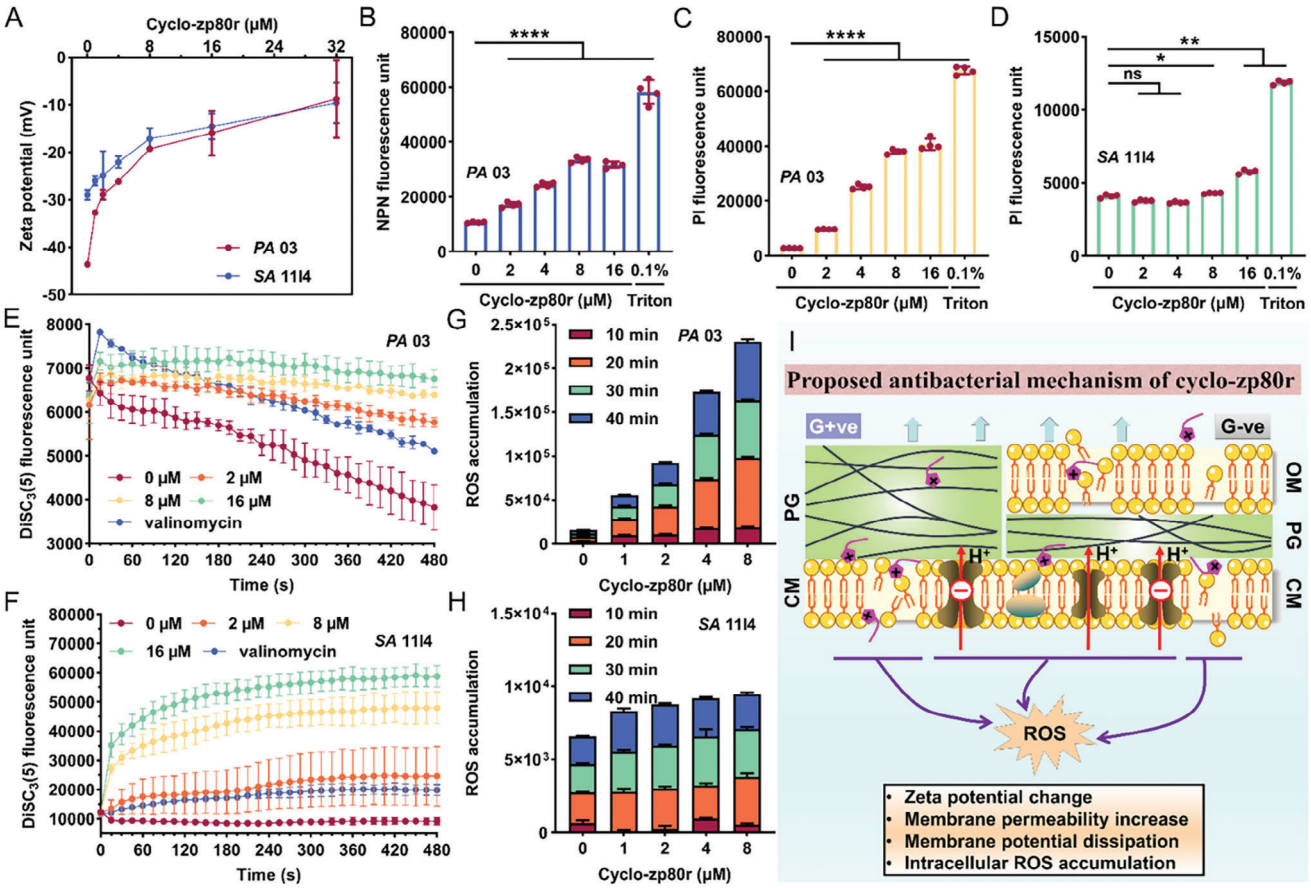


**Figure 5.** A) Zeta potential changes of *PA* 03 and *SA* 11I4; B) OM permeability of *PA* 03; CM permeability of *PA* 03 C) and *SA* 11I4 D); Membrane potential alteration of *PA* 03 E) and *SA* 11I4 F); ROS of *PA* 03 G) and *SA* 11I4 H). I) Schematic diagram of proposed antibacterial mechanism of **cyclo-zp80r**.

attention to modulate bacterial swarming behavior.[23] Our results verified that **cyclo-zp80r** could be an effective swarming inhibitor (Figure 4H). Swarming diameters decreased 35.4% for *PA* 03 and 44.4% for *SA* 11I4 in the presence of 8 μM **cyclo-zp80r**.

Collectively, **cyclo-zp80r**, like several host defence peptides, was able to kill persisters, destroy complex structure of biofilms, and inhibit swarming motility of *PA* 03 and *SA* 11I4 without inducing detected resistance. These data suggested that **cyclo-zp80r** could effectively overcome the common strategies adopted by bacteria to resist antibiotics, like persister cells formation and biofilm establishment.

### 2.4. Antibacterial Mechanism of cyclo-zp80r

The negatively-charged bacterial membrane was widely accepted as the paramount attacking sites for cationic peptides attributed to electrostatic attraction.[24] Zeta potential changes from more than –40 mV (*PA* 03) and nearly –30 mV (*SA* 11I4) to ≈ –10 mV, respectively in a dose-dependent manner clearly hinted that **cyclo-zp80r** could effectively interact with the negatively charged bacterial membrane via electrostatic and hydrophobic interactions (**Figure** 5A).

As a Gram-negative strain, *PA* 03 has an outer membrane (OM), conferring an advantage to evade the effects of antimicrobials.[25] The significant increase of 1-*N*-phenylnaphthylamine (NPN) fluorescence units suggested that **cyclo-zp80r** could permeablize the OM of *PA* 03 easily at the MIC, though less effecient than the well-known detergent Triton X-100 (Figure 5B). Furthermore, the cytoplasmic membrane (CM) permeability after **cyclo-zp80r** treatment was determined by propidium iodide (PI) staining. Likewise, **cyclo-zp80r** exhibited favorable activity in destroying CM of both *PA* 03 (Figure 5C) and *SA* 11I4 (Figure 5D). Typical fluorescent images of NPN or PI staining are shown in Figure S8 (Supporting Information). Though varied in membrane structure and thickness of the peptidoglycan (PG) layer, **cyclo-zp80r** seemed to be an effective cell-penetrating peptide that could reach the cytoplasm of both Gram-negative and Gram-positive strains.

Some antibiotics, like valinomycin, could modulate membrane potential, leading to imbalance of the concentration of cation inside and outside cells, thus affecting their normal physiological functions.[26] As depicted in Figure 5E, a treatment with **cyclo-zp80r** caused obvious membrane potential dissipation of *PA* 03 like the postive control valinomycin. To *SA* 11I4 cells, the potential alteration was more drastic (Figure 5F). During the first minute of drug treatment, the fluorescence units of $DiSC_3(5)$ rose sharply, indicating that the **cyclo-zp80r** molecules resulted in prompt cationic electrical turbulence across the phospholipid bilayers.

 

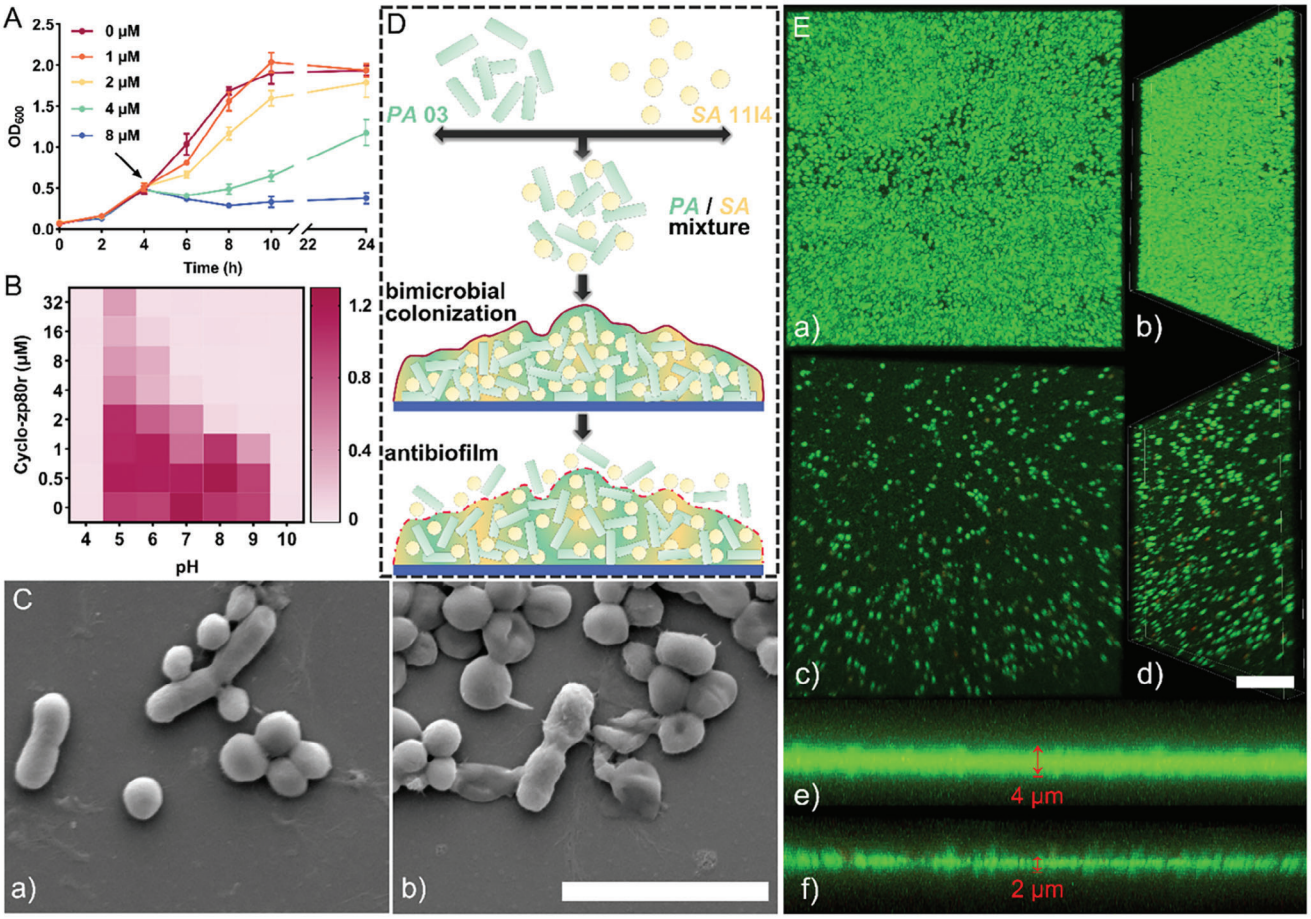


**Figure 6.** A) Bacterial growth curves of *PA* 03 and *SA* 1114 mixture in the presence of **cyclo-zp80r**; B) Antibacterial efficacy of **cyclo-zp80r** at different pH values; C) SEM images of *PA* 03 and *SA* 1114 mixture before (a) and after (b) **cyclo-zp80r** treatment. Scale bar: 4 μm; D) Schematic diagram of bi-microbial colonization; (E) *PA* 03 and *SA* 1114 bi-microbial biofilm visualization. Untreated in 2D (a) and 3D (b) format. **Cyclo-zp80r** treated in 2D (c) and 3D (d) format. Scale bar: 20 μm; Biofilm thickness evaluation before (e) and after (f) **cyclo-zp80r** treatment.

Accumulated reactive oxygen species (ROS) intracellularly could have irreversible effects on the survival of bacteria.[27] Herein, we analyzed oxidative stress levels of the two selected bacteria in the presence of **cyclo-zp80r**. For *PA* 03, **cyclo-zp80r** at 1 μM (1/2 MIC) could trigger significant ROS response. Within the monitor time, fluorescence units increased sharply after 10 min treatment for each test group, indicating that ROS begin to be produced in large quantities inside cytoplasm of *PA* 03 (Figure 5G). For *SA* 1114, ROS accumulation was not as significant as *PA* 03, but a clear dose-dependent effect could still be observed (Figure 5H).

The proposed antibacterial mechanisms of **cyclo-zp80r**, as outlined in Figure 5I, involves several key steps. First, positively-charged peptide interacted with *PA* and *SA* membranes via electrostatic attraction. Subsequently, the hydrophobic portion of this amphiphilic molecule may fuse with the phospholipid bilayer, allowing the **cyclo-zp80r** to penetrate inside and cause damage to it. During this process, membrane permeability increased and membrane potential dissipated. As a result, proton transport is affected, leading to the accumulation of intracellular ROS and subsequent cell death.

### 2.5. Efficacy of Cyclo-zp80r Combats Bi-Microbial Culture of PA and SA

Bi-microbial infections caused by *PA* and *SA* were frequently found in burn wound and cystic fibrosis.[28] Clinically, it has been reported to be associated with cystic fibrosis-induced decreased lung function.[29] Moreover, these two pathogens belong to Gram-negative and Gram-positive bacteria respectively. The effective killing of bi-microbial infection requires broad-spectrum antimicrobial agents. Thus, the efficiency of **cyclo-zp80r** in targeting the bi-microbial mixture of *PA* and *SA* was investigated. Bacterial growth curves of the *PA* 03 and *SA* 1114 coculture were revealed in **Figure 6**A. Initially, the OD values of the bacterial culture rose rapidly. After 4 h incubation, **cyclo-zp80r** at varied concentrations were added. Throughout the 24 h incubation period, the growth rate of the bacterial mixture was significantly decreased in a dose-dependent manner. As a horizontal comparison, at the same concentration of 8 μM, the inhibitory effect of **cyclo-zp80r** on bacterial coculture was better than the three commonly used antibiotics (Figure S9, Supporting Information). This result indicated that **cyclo-zp80r** could effectively restrain the proliferation of the tested bi-microbial culture.

As an arginine-rich peptide, the cationic charge of **cyclo-zp80r** is expected to be influenced by surrounding pH, jeopardizing its bioactivity. We therefore measured the antibacterial efficacy of **cyclo-zp80r** against the bi-microbial culture at different pH values. As shown in Figure 6B, bacterial cells failed to grow at pH 4 and 10 in the absence and presence of **cyclo-zp80r**, possibly accounted by the excessively acidic or alkaline environment. In the pH ranged 5 – 9, bacteria could grow efficiently and **cyclo-zp80r** could maintain its inhibitory performance against the *PA* 03 and *SA* 11I4 coculture, though mild compromisation was noted in a slightly acidic medium.

Bacterial cell deformation is usually a visual indication of the killing effect of a drug. Scanning electron microscopy (SEM) was then employed to observe the morphological changes of *PA* 03 and *SA* 11I4 coculture before and after the **cyclo-zp80r** treatment (Figure 6C). The morphology of *PA* 03 (rod shape) and *SA* 11I4 (round shape) cells treated with **cyclo-zp80r** were both distinct from healthy ones. For *PA* 03, shrinkage and fragmentization could be observed. For *SA* 11I4, obvious concaves and holes were captured. These abnormal morphological features, together with above molecular biological assays, collectively proved that **cyclo-zp80r** triggered multiple cellular dysfunction and rapid cell death.

As mentioned above, bacterial cells are prone to generate extracellular polymeric substances to form a biofilm and embedded themselves within to resist antibacterial agents. Composite biofilm, secreted by polymicrobial colonization, is even harder to eliminate. Typically, the co-existence of *PA* and *SA* could lead to dual-species bacterial biofilms. Here, an in vitro *PA* 03 and *SA* 11I4 bi-microbial biofilm model was established and the antibiofilm activity of **cyclo-zp80r** was evaluated. Figure 6D shows a schematic diagram biofilm co-establishment by *PA* 03 and *SA* 11I4. It is noteworthy to highlight that it is a dynamic process to culture the two bacteria strains together with their ratio constantly changing throughout the incubation period (Figure S10, Supporting Information). After 24 h incubation, the *PA* 03: *SA* 11I4 ratio was ≈65%:35%, which was basically consistent with a previous study that *PA* would be the dominant species during the coevolution with *SA*.[30] According to the 2D (**a** of Figure 6E) and 3D (**b** of Figure 6E) confocal images, a compact bi-microbial biofilm was successfully established. Z-axis scanning confirmed that the untreated biofilm thickness was ≈4 µm (**e** of Figure 6E). After incubation with **cyclo-zp80r**, the biomass of biofilm reduced remarkably (**c** and **d** of Figure 6E). Meanwhile, the average thickness of **cyclo-zp80r**-treated biofilm decreased to 2 µm (**f** of Figure 6E). These data were consistent with the efficacy against the single-species biofilm shown in Figure 4E,G. Collectively, **cyclo-zp80r** demonstrated excellent antibiofilm capacity of destroying the structure of the bi-microbial biofilm and killing the enclosed bacterial cells.

### 2.6. Formulation Study of Hydrogel-Encapsulated Cyclo-zp80r (HEP)

The co-infection of *PA* and *SA* is prevalent in chronic wounds, which can express virulence factors and impede wound healing, demonstrating more virulent than single infection.[31] The efficiency and compatibility of biomaterials would be important evaluation indicators for managing infected wound.[32] To maximize the therapeutic potential of **cyclo-zp80r** in managing skin infections associated with polymicrobial colonization, we next developed the peptide into an in situ hydrogel wound dressing. Maintaining liquid status at room temperature while gelling at human skin temperature is a desired feature for thermosensitive hydrogels.[33] Since the interactions between incorporated agents and the polymer networks are often drug-specific, an elaborate formulation study was launched to develop a hydrogel wound dressing for this new compound **cyclo-zp80r**.

**Table 2.** Compositions and gelling temperatures of hydrogel formulations.

| Formulation | P407 [%] | P188 [%] | HA [%] | Gelling temperature [°C] |
|---|---|---|---|---|
| F1 | 20 | 1 | 0.2 | 27 |
| F2 | 20 | 3 | 0.15 | 37 |
| F3 | 22 | 5 | 0.15 | 33 |
| F4 | 20 | 3 | 0.15 | 37 |
| F5 | 22 | 1 | 0.15 | 24.5 |
| F6 | 20 | 3 | 0.15 | 37 |
| F7 | 18 | 3 | 0.1 | 47.5 |
| F8 | 18 | 3 | 0.2 | 47.5 |
| F9 | 20 | 1 | 0.1 | 28 |
| F10 | 20 | 5 | 0.1 | 41 |
| F11 | 18 | 1 | 0.15 | 32.5 |
| F12 | 22 | 3 | 0.1 | 28 |
| F13 | 20 | 5 | 0.2 | 40.5 |
| F14 | 18 | 5 | 0.15 | 52.5 |
| F15 | 20 | 3 | 0.15 | 36.5 |
| F16 | 20 | 3 | 0.15 | 37 |
| F17 | 22 | 3 | 0.2 | 27.5 |

In this study, poloxamer 407 (P407) and 188 (P188) were chosen as critical components of the hydrogel because they are safe and readily available pharmaceutical excipients with excellent thermosensitive characteristics.[34] In general, the mechanical strength of the hydrogels solely composing of poloxamers-only may not be sufficient to allow firm attachment to the skin surface. In this regards, hyaluronic acid (HA) was added to the formulationto promote the adhesiveness of the hydrogel.[35] In addition, the moisturizing property of HA is expected to accelerate wound healing, making the hydrogel system more suitable for treating wound infections.[36] **Figure 7A** depicts the hydrogel system developed for **cyclo-zp80r**. A Box-Behnken design of experiments (DOE) approach was adopted to optimize the formulation with desirable gelling temperatures ($T_{gel}$). **Table 2** shows the compositions and $T_{gel}$ of 17 formulations investigated. Empirically, the increase of P407 content reduced the $T_{gel}$ mildly. On the contrary, the increase of P188 content led to a sharp rise in $T_{gel}$. Among the range of 0.1% – 0.2%, the influence of HA on $T_{gel}$ was insignificant. The response surface curve illustrated in Figure 7B intuitively showed the impact of changes in composition on $T_{gel}$. Among all prepared formulations, F3 and F11 were considered to be appropriate since they gelled at 33 and 32.5 °C, respectively, just slightly below the average skin temperature 34 °C. Compared to F3 (22% P407, 5% P188, and 0.15% HA), F11 required less raw

 

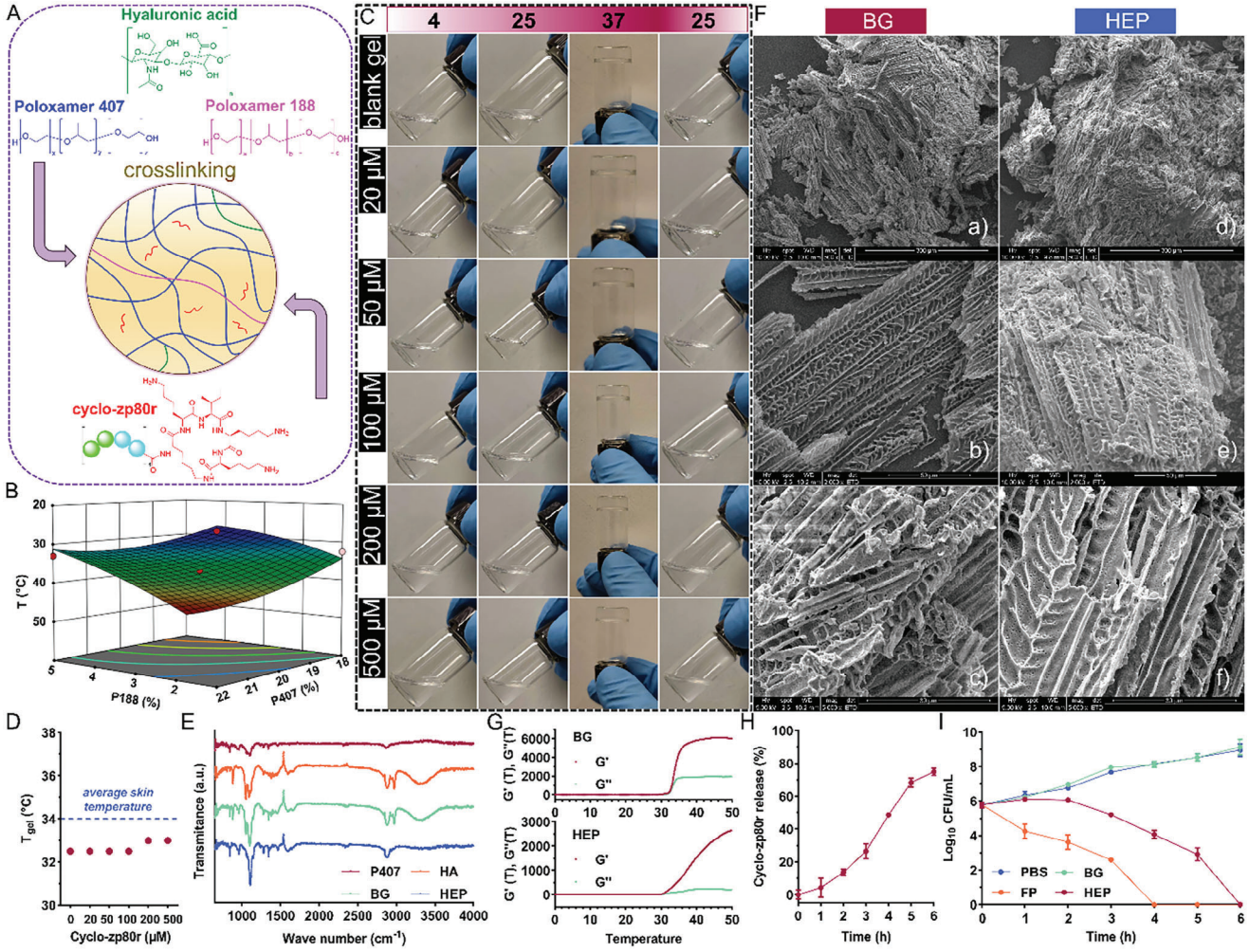


**Figure 7.** A) Schematic diagram of ternary hydrogel; B) Response surface curve of these hydrogel formulations; C) Thermosensitivity test of F11 in a 4 °C-25 °C-37 °C-25 °C cycle in the absence/presence of **cyclo-zp80r**; D) $T_{gel}$ of **cyclo-zp80r**-loaded hydrogels; E) FTIR spectra of P407, HA, BG, and HEP; F) SEM images of lyophilized BG and HEP at 500-fold (a and d), 2000-fold (b and e) and 5000-fold (c and f) magnification; G) Temperature dependence of storage modulus (G′) and loss modulus (G″) for BG and HEP; H) Release curve of **cyclo-zp80r**; I) Time-killing kinetics against *PA* 03 and *SA* 1114 mixture.

materials (18% P407, 1% P188, and 0.15% HA). Therefore, F11 was selected for further study.

After determining the most suitable formulation composition, **cyclo-zp80r** was incorporated into this ternary hydrogel for further testing (Figure 7C). Like blank gel, hydrogels containing **cyclo-zp80r** from 20 to 500 μM exhibited similar liquid-solid-liquid transformation in a 4 °C-25 °C-37 °C-25 °C cycle, indicating that the thermosensitivity would not be affected over a wide range of **cyclo-zp80r** concentrations. $T_{gel}$ of the **cyclo-zp80r** incorporated hydrogels were determined (Figure 7D). Only a slight increase in $T_{gel}$, from the original 32.5 to 33 °C, was noted when ≥200 μM **cyclo-zp80r** was added. It is worth noting that in the presence of >200 μM **cyclo-zp80r**, the hydrogel started to become turbid. However, it was still a stable system with no precipitation observed after storing at 4 °C for a month.

Fourier transform infrared spectroscopy (FTIR) spectra revealed interactions between different components within the hydrogel system (Figure 7E). In general, P407 is compatible with HA, for absorption peaks of these two regions have a certain degree of superposition in the cross-linked blank gel (BG). Notably, a broad hydroxyl absorption peak at ≈ 3000 – 3500 $cm^{-1}$ diminished in HEP based on F11, indicating the formation of intermolecular hydrogen bonds. Moreover, lyophilized hydrogel powder, no matter BG or HEP, displayed regular porous structures (**a** and **d** of Figure 7F). This orderly-packed solid gel with channel-like lamellar framework allowed the diffusion of hydrophilic peptides, like **cyclo-zp80r**, from the polymeric network. From the appearance imaged by SEM, the presence of **cyclo-zp80r** had no impact on the size or distribution of pores (**b** and **e** of Figure 7F). At 5000-fold magnification, more fine pores can be observed (**c** and **f** of Figure 7F), which could be very conducive to the movement of encapsulated antibacterial molecules throughout the hydrogel.

Since this hydrogel was thermosensitive, its rheological properties regarding temperature dependence of storage modulus and loss modulus were thus measured (Figure 7G). It can be

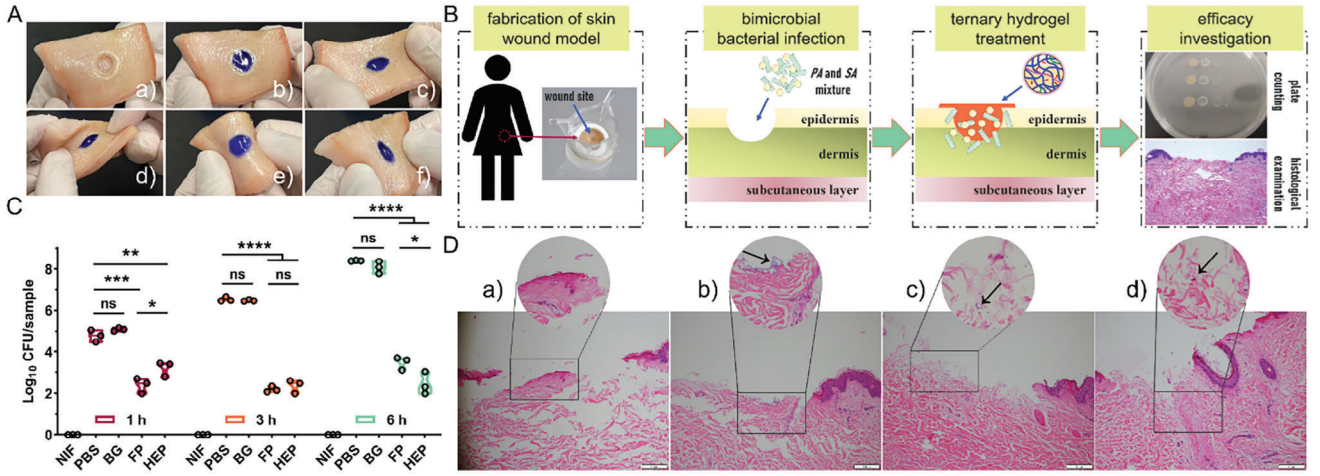


**Figure 8.** A) Mechanical pressure test of hydrogel in pork skin. (a) fabrication of wound, (b) gel injection, (c) stretching, (d) twisting, (e) bending, (f) compressing. Hydrogel was stained by crystal violet for better visualization; B) Schematic diagram of human skin model; C) Bacterial counting for skin tissues; D) Histological examinations of wounded skin tissues. (a) non-infected, (b) PBS-treated, (c) FP-treated, (d) HEP-treated. The black arrows indicate bacterial cells adhere to the wound surface.

found that, at temperature range lower than 30 °C, the storage and loss moduli (G′ and G″) exhibited small magnitude no matter in the absence or presence of peptide **cyclo-zp80r**. However, near the critical point of transition, these parameters increased drastically, suggesting the rapid gel forming process. The reversible gelation process indicated dynamic changes between individual polymer chains to aggregates and this equilibrium would not be affected by the presence of **cyclo-zp80r**.

The release profile of HEP was then investgated (Figure 7H). Within the first 3 h, ≈30% of **cyclo-zp80r** was released from the hydrogel. In the next 3 h, the release rate increased slightly to reach 74.93% at the 6 h timpoint, achieving a sustained release of the incorporated peptide. Next, we examined the time-killing kinetics of PBS, BG, free peptide (FP) and HEP (Figure 7I). For control groups, bacterial counts of the bi-microbial culture treated with PBS and BG increased steadily from 6 log to 9 log synchronously, suggesting that the hydrogel itself had no antibacterial activity. For the free peptide (FP) group, which **cyclo-zp80r** was directly added into the bacterial solution, no bacterial colony was detected after 4 h treatment. When equivalent peptide was loaded into the hydrogel, a slower killing kinetics was observed compared with the FP group. However, it was still able to eliminate *PA*03 and *SA* 11I4 mixture within 6 h, consistent with the release profile shown in Figure 7H.

### 2.7. Ex vivo Study of Wound Skin Models

Then, the hydrogel was applied to *ex vivo* skin models to evaluate its practical feasibility. A wound was artificially created on the surface of the pig skin using a biospy punch (**a** of **Figure** 8A). Subsequently, the liquid hydrogel was injected into the wound site at room temperature and transferred to 37 °C for gelling. The thermosensitive gel could nicely filled the whole wound and formed a rigid hydrogel (**b** of Figure 8A). After that, the pig skin was subjected to stretching (**c** of Figure 8A), twisting (**d** of Figure 8A), bending (**e** of Figure 8A), and compressing (**f** of Figure 8A). Inflicting external forces would not cause the hydrogel to crack or detach, verifying its applicability as topical wound dressing.

Next, human skin, a model closer to the real application, was employed to investigate the antibacterial activity of HEP (Figure 8B). Skin tissues were taken from abdomen during a surgical procedure and a wound was fabricated thereafter. After bi-microbial infection (*PA* 03 and *SA* 11I4), the hydrogel solution was injected to the wound site at 37 °C. The antibacterial efficacy was then determined by plate counting at three selected time points (1, 3, and 6 h after treatment) (Figure 8C). The dynamic changes of bi-microbial infection under different treatment was successfully captured. For tissues treated with PBS and BG, bacterial colonies gradually increased by ≈3 log in 6 h, indicating that bacterial cells proliferated quickly on wounds in nutrient-rich human tissue. Meanwhile, no statistical difference was found between the two control groups at all three sampling time points, further proving that the hydrogel alone had no antibacterial effect. In contrary, infected wounds treated with FP and HEP showed significant decrease of bacterial colonies at 1 h. Over the next 5 h, **cyclo-zp80r** maintained a sustained inhibitory effect. Notably, FP demonstrated better antibacterial activity at 1 h compared to HEP. This is reasonable because FP was readily available to interact with the infected skin tissue and kill bacteria in the early stages. While at 3 h, there was no significant difference between FP and HEP groups. After 6 h treatment, viable bacterial cells of the FP group started to show an upward trend, but the HEP group still kept at a relative low level. This is another proof that the sustained release nature of the designed hydrogel could extend the treatment period to achieve better therapeutic outcome than free drug. The measurement after 6 h treatment revealed that the number of viable bacteria in PBS and BG groups were more than 10000-fold higher (>4 logs) than that of FP and HEP groups. As negative controls, no colony was detected for the non-infected (NIF) skin tissues throughout the experimental period.

Histological sections at wound sites were examined. Partial missing of epidermis validated the formation of wound for all

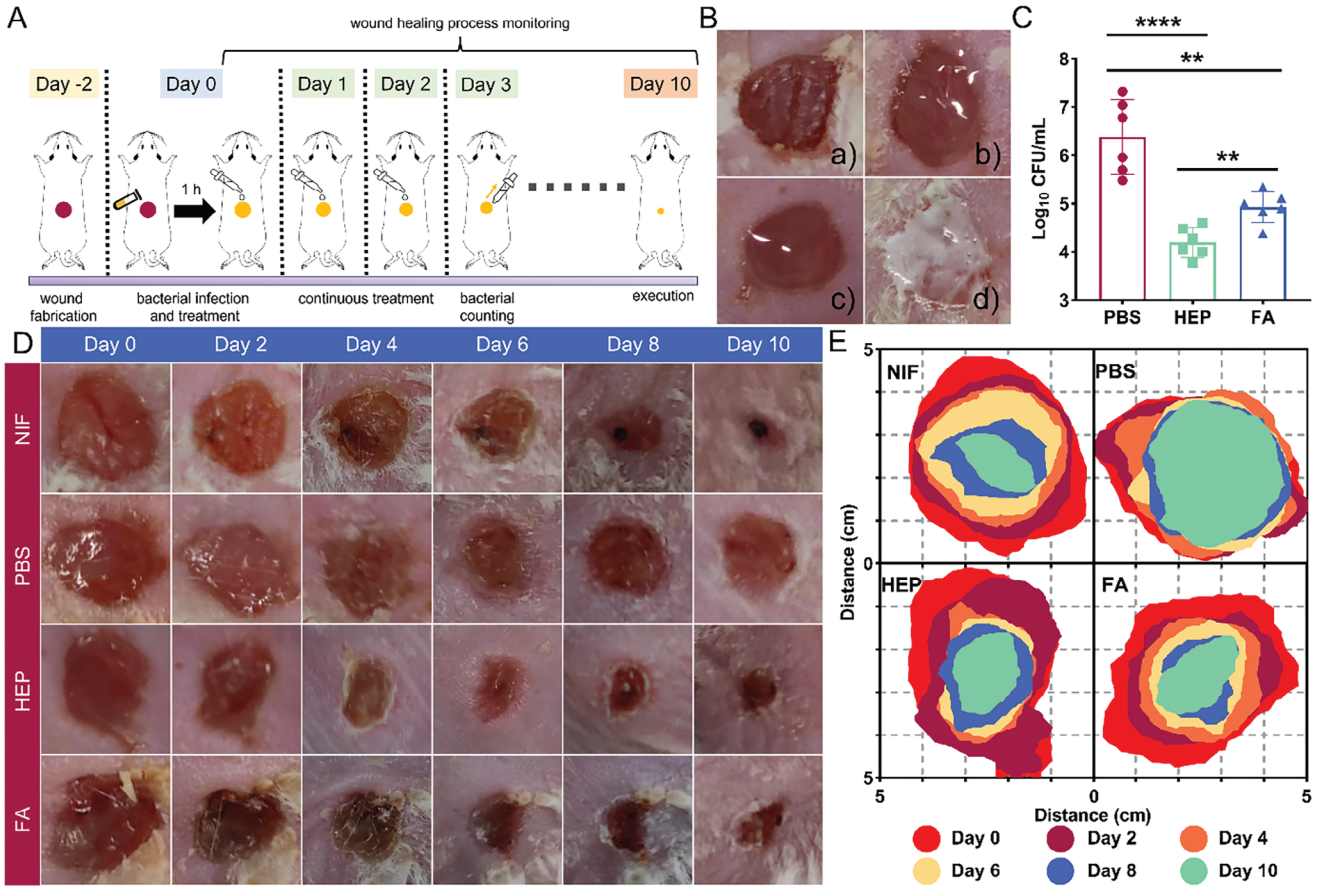


**Figure 9.** A) Schematic diagram of mouse wound infection model. B) Images of wound sites. (a) dry wound with no infection, (b) PBS treatment, (c) HEP treatment, (d) FA cream treatment. C) Bacterial counting for wound sites. D) Typical images of wound healing process. E) Wound size change with time.

tested tissues (Figure 8D). Besides that, no abnormal structure or morphology was observed in NIF group, suggesting that it was a healthy skin tissue (**a** of Figure 8D). However, at the wound site of the PBS-treated tissue, a large number of bacterial cells can be seen (**b** of Figure 8D). After **cyclo-zp80r** treatment, in both FP (**c** of Figure 8D) and HEP (**d** of Figure 8D) groups, the number of observable bacteria decreased significantly, although sporadic cells may invade deep into the tissues.

### 2.8. In Vivo Study of Eliminating Skin Infections and Promoting Wound Healing in a Mouse Wound Infection Model

Finally, the in vivo effect of this ternary hydrogel was verified using a mouse model (**Figure 9A**). Wounds in the shaved back skin of mice were fabricated by punch biopsy two days to ensure no more no tissue exudation from the punctured site (**a** of Figure 9B) before infecting by a *PA* ($\sim 10^4$ CFU) and *SA* ($\sim 10^4$ CFU) mixture. One hour post-infection, mice were randomized to be treated with PBS, HEP or commercial available fusidic acid (FA) cream (2%) for three consecutive days. FA cream is mainly for *SA* infection clinically, which would be its limitation in treating bi-microbial colonization. When dropping PBS (**b** of Figure 9B) or F11 hydrogel (**c** of Figure 9B) into the wound, both liquids can spread spontaneously to cover the wound evenly. While overflown of PBS solution from the wound site was observed due to its low viscosity, HEP quickly solidified to form a rigid gel. As a semi-solid, FA cream was applied to the wound bed by smearing (**d** of Figure 9B). Figure 9C compared the number of bacterial cells of wounds treated with PBS, HEP and FA after three consecutive days therapeutics. The bacterial burden of the HEP group was averagely reduced by >2 logs. Encouragingly, it exhibited improved in vivo antibacterial efficacy compared to the FA group in this bi-microbial infection system.

As a functional biomaterial, hydrogel has show attractive advantages in promoting wound healing.[37] Herein, we monitored the change of wound area for 10 days. These real wound images suggested that bacterial infection caused by *PA* 03 and *SA* 11I4 mixture could significantly slow the healing of wounds (Figure 9D). At 10 day post-infection, wound size of PBS-treated mice shrinked only ≈ 30% (Figure 9E). As a comparison, treating infected area with HEP or FA helped to reduce the size of >70% and ≈60%, respectively. Statistically, mice in the HEP groups healed faster than those in the PBS group (Figure S11, Supporting Information). For most newly designed hydrogels, their application is limited to single bacterial infection. While these data hinted that **cyclo-zp80r** could release from the proposed ternary thermosensitive hydrogel

system and reduce the bacterial load of *PA* and *SA* co-infection effectively.

## 3. Conclusion

In conclusion, we have designed and synthesized a promising cyclic peptide termed **cyclo-zp80r** in this study. It shows a broad antibacterial spectrum against both Gram-negative and Gram-positive strains, especially for many clinical isolates and drug-resistant superbugs. Peptide **cyclo-zp80r** exerts antibacterial activity by interacting with the negatively-charged cellular membrane to cause potential dissipation, resulting in electron transport chain inhibition and aberrant accumulation of ROS. For controlling the bi-microbial colonization of *PA* and *SA*, **cyclo-zp80r** exhibits favorable bioactivities against bacteria at both planktonic and biofilm states.

To treat open wounds with bi-microbial bacterial infections effectively, we developed a ternary thermosensitive hydrogel formulation. It is composed of P407, P188 and HA with the mass fraction of 18%, 1%, 0.15%, respectively. This porous hydrogel was further verified as an appropriate system for delivering **cyclo-zp80r** in a slow-release manner. This hydrogel could stand moderate mechanical pressure after gelling on the skin surface without slide away or being destroyed. Encapsulated **cyclo-zp80r** molecules could release in a sustain manner to eliminate epidermal bi-microbial colonization.

Collectively, a systematical research from design and chemical synthesis of a novel cyclic peptide, a antibacterial mechanism study and formulation optimization for topical wound infection were completed herein. Proposed therapeutics could be a promising strategy to treat bi-microbial wound infections.

## 4. Experimental Section

*Peptide Synthesis*: All peptides were customized by Synpeptide Co., ltd (Nanjing, China). The crude product was purified using HPLC (Agilent Technologies, USA) to >90% purity.

*Antibacterial Activity, Cytotoxicity, and Hemolysis Test—Bacterial Strains*: Standard strains were purchased from ATCC. Clinical isolates were from our in-house stock.

*MIC Determination*: MIC values were determined by double-dilution method as previous protocol.[38] Briefly, freshly-prepared logarithmic bacterial cells were diluted to $OD_{600}$ value of 0.1. Then, a total of 5 µL cell suspension was mixed with 150 µL of Mueller Hinton broth (MHB, Hopebio, China) medium containing tested peptides at various concentrations. After 18 h treatment, the lowest concentration showed no observed turbidity was defined as the MIC.

*Cytotoxicity*: HaCaT cells incubated in vitro with Dulbecco's modified eagle medium (DMEM, HyClone, USA) were treated with **cyclo-zp80r** at various concentrations for 24 h. Then, a volume of 20 µL of thiazolyl blue tetrazolium bromide (MTT, Sigma-Aldrich, USA) at 5 mg $mL^{-1}$ for further 4 h. Then, medium was removed and the precipitated formazan was dissolved in 150 µL of dimethylsulfoxide (DMSO, Dieckmann, Hong Kong). The $OD_{570}$ values were tested by a microplate reader (Clariostar, BMG Labtech, Germany). Survival ratio was defined as the $OD_{570}$ values of **cyclo-zp80r**-treated groups versus the phosphate-buffered saline (PBS, Solarbio, China)-treated group, which was considered as 100%. Three biological replicates were performed.

*Hemolysis Test*: Fresh rat blood was centrifuged and only RBCs were kept. RBCs were washed with PBS thrice and finally diluted to 8%. Peptides **zp80r** and **cyclo-zp80r** at various concentrations were added to treat them for 1 h respectively. Then, RBCs were centrifuged for 5 min. The supernatant was transferred to a 96-well plate to measure their $OD_{540}$ values. RBC groups treated with PBS and 0.1% Triton X-100 (Solarbio, China) were set as negative control (0% hemolysis) and positive control (100% hemolysis). Three biological replicates were performed.

*Growth Curve*: Bacterial solutions of *PA* 03 and *SA* 11I4 containing **cyclo-zp80r** at various concentrations were prepared following the MIC determination protocol abovementioned. $OD_{600}$ values were recorded every 2 h, lasting 24 h, by a microplate reader (Clariostar, BMG Labtech, Germany). Three biological replicates were performed.

*Time-Killing Curve*: *PA* 03 and *SA* 11I4 cells at logarithmic phase were diluted to the CFUs ≈ $10^5$ – $10^6$ $mL^{-1}$. Next, bacterial cells were treated with PBS, 2, 8, and 16 µM **cyclo-zp80r** respectively at 37 °C. Every 1 h, a total of 100 µL aliquots for each group were pipetted to a 96-well plate and diluted by PBS in a continuous tenfold dilution assay. Prepared samples were dropped on the surface of MHA plates. After overnight incubation, visible bacterial colonies were counted and the original CFU/mL was calculated accordingly. *PA* 03 treated with 16 µM of colistin and SA 11I4 treated with 16 µM of vancomycin were set as positive controls. Three biological replicates were performed.

*MBC Determination*: Bacterial cells (*PA* 03 and *SA* 11I4) with the initial concentration of 5 × $10^5$ CFU $mL^{-1}$ were treated with **cyclo-zp80r** for 18 h. A volume of 10 µL bacterial solution was dropped on the MHA plates for observation. MBC values were defined as the lowest concentration that can reduce the number of colony by 3 logs (99.9%) compared to non-treated control group.

*Proteolytic Stability and Structural Prediction—Trypsin Tolerance*: For MIC fold change test, all steps were the same as the MIC determination protocol except additional trypsin (HyClone, USA) from 0.03 – 4 µg $mL^{-1}$ were added.

For quantitative degradation test, **cyclo-zp80r** solution at 100 µM was treated with 4 µg $mL^{-1}$ trypsin (HyClone, USA) at room temperature. The samples were analyzed using HPLC (Agilent Technologies, USA) at 2 h intervals. The degree of degradation was calculated by the ratio of two integral areas at 0 h (set as 100%) and 6 h.

*Serum Tolerance*: FBS was purchased from HyClone, USA. *PA* 03 and *SA* 11I4 cells at logarithmic phase were collected by centrifugation and resuspended in different MHB/FBS mixtures with initial $OD_{600}$ at 0.1. Cells were then seeded in a 96-well plate and 5 µM **cyclo-zp80r** was added for each well. After 8 h incubation, $OD_{600}$ values were recorded.

*CD Spectroscopy and Structural Prediction*: Peptide **cyclo-zp80r** was dissolved in deionized water and 50 mM SDS (Tokyo Chemical Industry, Japan) repectively with the final concentration of 0.05 mM. Signals were measured at wavelengths between 190 and 260 nm by a J-1500 CD spectrometer (Jasco, Japan). The mean residue ellipticity $[\theta]$ was determined as $[\theta] = [\theta]_{obs}$ / 10rlc ($[\theta]_{obs}$: measured data, r: number of amino acid residue, l: optical path of sample cell, c: concentration of **cyclo-zp80r**). The ratio of secondary structure was predicted by BeStSel (https://bestsel.elte.hu/index.php).[39]

PEP-FOLD 4 server (https://bioserv.rpbs.univ-paris-diderot.fr/services/PEP-FOLD4/) was used to visualize the structures of **cyclo-zp80r**.[40] After inputting the linear sequence of $(IIRR)_4$KKIKK, the PDB file of the best model was downloaded. Since current version only supports natural amino acids, the L-arg residues were edited manually to D-arg, and the cyclic part was edited to form a ring. It was then subjected to energy minimization by using MM2 calculation of Chem3D to obtain the predicted structure.

*Activity Against Persister, Biofilm, Swarming, and Resistance Development—Persister Sensitivity*: *PA* 03 and *SA* 11I4 cells at logarithmic phase were collected and resuspended in 0.9% NaCl (Dieckmann, Hong Kong) solution for 72 h starvation at 4 °C. Then, MIC values of **cyclo-zp80r**, colistin (≥19 000 U $mg^{-1}$, Meryer, China) and vancomycin (≥900 µg $mg^{-1}$, Sigma–Aldrich, USA) against normal cells and persisters were determined following the protocol abovementioned.

*Resistance Development*: The $OD_{600}$ values of *PA* 03 and *SA* 11I4 bacterial suspensions were adjusted to 0.1. Then, cells were diluted 30-fold in MHB. Colistin and **cyclo-zp80r** were subsequently applied to *PA* 03 at their respective 1/2 MIC. Meanwhile, vancomycin and **cyclo-zp80r** were

applied to *SA* 1114 at their respective 1/2 MIC. After 12 h of incubation, cells were collected, cryopreserved and their MICs were determined at the same time. Cryopreserved strains were regarded as passage 1. Next, this process was reiterated with continuous updated MICs until passage 20.

*Antibiofilm Activity*: Inhibiting biofilm formation test. *PA* 03 and *SA* 1114 cells at logarithmic phase were adjusted to $OD_{600}$ at 0.1 respectively. Then cells were diluted 30-fold in MHB and seeded in a 96-well plate. Peptide **cyclo-zp80r** at different concentrations (1 – 16 μм) were applied to treat them for 18 h. Planktonic cells were removed and the wells were rinsed three times. Next, biofilms were stained with 0.1% crystal violet solution for 30 min. After rinsing the unbound dye, a volume of 150 μL of absolute ethanol was used to dissolve the sediment adequately. The $OD_{595}$ values were measured and the cells without **cyclo-zp80r** treatment was defined as 100% biomass of biofilm.

Eliminating preformed biofilm test. *PA* 03 and *SA* 1114 cells were incubated in a 96-well plate for 3 days to form a solid biofilm. Then, planktonic bacteria were removed, and **cyclo-zp80r** at various concentrations (2 – 32 μм) were applied to treat these preformed biofilms for 12 h. Finally, biomass of biofilm was determined by crystal violet assay as above.

Preformed bacterial biofilms (*PA* 03 and *SA* 1114) were treated with PBS and 2 – 32 μм of **cyclo-zp80r** for 6 h. After rinse, remaining biofilms were stained with 0.1% crystal violet solution for 30 min, and then filmed by a live-cell imaging system in bright field (Nikon Eclipse Ti2-E, Japan).

*Bacterial Swarming Test*: The swarming test was performed in double-layer semisolid agar plate. 1.5% nutrient agar plates (Sigma-Aldrich, USA) were prepared in advance. Next, 0.5% pure agar (Sigma-Aldrich, USA) containing 0 – 8 μм **cyclo-zp80r** was poured atop. Then, a volume of 10 μL bacterial solutions of *PA* 03 and *SA* 1114 ($OD_{600}$ = 0.1) were dropped on the center of the plate. Images were filmed by ChemiDoc Imager (Bio-Rad, USA) after 48 h incubation. The diameters of bacterial swarming distances were recorded.

*Mechanistic Study—Zeta Potential*: *PA* 03 and *SA* 1114 cells at logarithmic phase were centrifuged and resuspended in PBS to $OD_{600}$ at 0.2 respectively. Then, **cyclo-zp80r** at various concentrations (0 – 32 μм) were applied to treat cells for 10 min. Zeta potential of each group was measured by Delsa Nano C particle analyzer (Beckman Coulter, USA).

*OM Permeability*: *PA* 03 cells at logarithmic phase were treated with **cyclo-zp80r** at various concentrations (2 – 16 μм) for 1 h. Cells treated with PBS and 0.1% Triton X-100 (Solarbio, China) were set as two control groups. Subsequently, 10 μм NPN (Sigma-Aldrich, USA) was applied to stain the tested bacterial suspensions for 5 min. Fluorescence units were then recorded with an exciting wavelength at 350 nm and an emission wavelength at 420 nm by a microplate reader (Clariostar, BMG Labtech, Germany).

*CM Permeability*: *PA* 03 and *SA* 1114 cells at logarithmic phase were treated with **cyclo-zp80r** at various concentrations (2 – 16 μM) for 1 h, respectively. Cells treated with PBS and 0.1% Triton X-100 (Solarbio, China) were set as two control groups. Then, 10 μg $mL^{-1}$ PI (Thermo Fisher, USA) was incubated with the bacterial suspensions for another 20 min. Fluorescence units were recorded with an exciting wavelength at 535 nm and an emission wavelength at 615 nm by a microplate reader (Clariostar, BMG Labtech, Germany).

*Membrane Potential*: *PA* 03 and *SA* 1114 cells at logarithmic phase were adjusted to $OD_{600}$ = 0.1 in PBS, respectively. Cells were then incubated with 0.5 μм $DiSC_3(5)$ (Invitrogen, USA) for 1 h. After rinse, **cyclo-zp80r** at various concentrations (2 – 16 μм) was added. Cells treated with PBS and 5 μм valinomycin (Sigma-Aldrich, USA) were set as two control groups. Fluorescence units were recorded immediately every 15 s with an exciting wavelength at 622 nm and an emission wavelength at 670 nm by a microplate reader (Clariostar, BMG Labtech, Germany).

*ROS Accumulation*: *PA* 03 and *SA* 1114 cells at logarithmic phase were resuspended in PBS with $OD_{600}$ = 0.6, respectively. Cells were then incubated with 10 μм 2,7-dichlorodi-hydrofluorescein diacetate (DCFH-DA, Thermo Fisher, USA) for 30 min. Subsequently, they were treated with 1 – 8 μм **cyclp-zp80r**, and PBS-treatment was defined as the control. Every 10 min, fluorescence units were recorded with an exciting wavelength at 488 nm and an emission wavelength at 525 nm by a microplate reader (Clariostar, BMG Labtech, Germany), lasting for 40 min.

*Bi-Microbial Test—Growth Curve of Bi-Microbial Culture*: *PA* 03 and *SA* 1114 cells were adjusted to $OD_{600}$ = 0.1, respectively. These two bacterial suspensions were mixed with the volume ratio of 1:1. Prepared bi-microbial culture was seeded in a 96-well plate and incubated at 37 °C for 4 h. Then, **cyclo-zp80r** at various concentrations (1 – 8 μм) were added. Their $OD_{600}$ values were constantly monitored for 24 h.

*Antibacterial Efficacy at Different pH Values*: Sterile MHB solutions were divided into seven groups. Their pH values were adjusted to 4 – 10 using hydrochloric acid or sodium hydroxide. Prepared bi-microbial cultures as above were resuspended in these pH-varied medium respectively with the initial $OD_{600}$ = 0.1. Then, **cyclo-zp80r** at various concentrations (0.5 – 32 μм) were added to incubate for 6 h. The final $OD_{600}$ values were recorded by a microplate reader (Clariostar, BMG Labtech, Germany).

*Bi-Microbial Morphology*: *PA* 03 and *SA* 1114 cells were adjusted to $OD_{600}$ = 0.6, and mixed with the volume ratio of 1:1. Then, the bi-microbial cultures were treated with PBS or 5 μм **cyclo-zp80r** for 4 h, respectively. Afterward, they were resuspended in 2.5% glutaraldehyde (Tokyo Chemical Industry, Japan) overnight at 4 °C for fixation. Then, two samples were subjected to a dehydrated process through a graded ethanol series (50, 70, 90, and 100%). A volume of 2 μL bi-microbial sample was dropped onto a clear coverslip. After air-drying, and platinum coating, pictures were finally taken by a SEM (FEI Quanta 400F, Netherland).

*Bi-Microbial Biofilm Eradication*: *PA* 03 and *SA* 1114 cells were adjusted to $OD_{600}$ = 0.1 in MHB, and mixed with the volume ratio of 1:1. A sterile coverslip was placed on the bottom of a petri dish. Prepared bi-microbial culture was then transferred to it, allowing the accumulation of biofilm on this coverslip. 3 days later, planktonic bacteria were gently removed, and PBS or 10 μм **cyclo-zp80r** were applied to treat these preformed biofilms for 6 h. Next, LIVE/DEAD BacLight Bacterial Viability dye prepared according to kit specification (Molecular Probes, USA) was used to stain the bi-microbial biofilm for 20 min. After that, two coverslips were washed with PBS and filmed by a confocal microscope (Leica TCS SPE, Germany).

*Formulation Study—Hydrogel Preparation*: Formulation strategies were generated by the sofeware Design of Experiments 12. Powder mixtures of P407, P188, HA, and **cyclo-zp80r** were dissolved in deionized water to prepare polymer solutions. They were slightly oscillated at 4 °C for at least 48 h for complete hydration. Prepared samples were stored at 4 °C.

*Thermo Sensitivity Test*: $T_{gel}$ was determined by the tilt method. In brief, a volume of 1 mL gel solution was transferred into a glass vial and placed in a water bath at a set temperature for 1 min. Then, the vial was taken out and tilted to check the flowability. Testing temperatures ranged from 22 – 53 °C at an increment of 0.5 °C. The lowest temperature at which the solution completely solidifies was defined as $T_{gel}$.

*FTIR*: Powders of P407, HA, and lyophilized hydrogels were combined with KBr (optically pure, Sigma-Aldrich, USA), respectively. They were then ground and pressed into tablets. Spectra of the wavenumber from 650 – 4000 $cm^{-1}$ were obtained using the FTIR spectrophotometer (Nicolet, Thermo Fisher, USA).

*Hydrogel Morphology*: Liquid solutions of F11 blank hydrogel and 200 μм **cyclo-zp80r**-containing F11 hydrogel were solidified at 37 °C. Then, they were rapidly immersed in liquid nitrogen for 60 min. Frozen gels were transferred to the vacuum freeze dryer to lyophilization for three days. The freeze-dried powders were affixed to a carbon tape, coated with platinum and imaged by a SEM (FEI Quanta 400F, Netherland).

*Rheological Property*: F11 blank hydrogel and 200 μм **cyclo-zp80r**-containing F11 hydrogel were prepared as above. The rheology of samples were tested by a rheometer (Haake Mars 40, Germany) adopting oscillatory measurement mode with constant strain of 1% and contant frequency of 1 Hz. The temperature increased by 1 °C $min^{-1}$ from 0 to 50 °C.

*Peptide Release*: The gel (1 mL) containing 200 μм **cyclo-zp80r** was solidified in a tube at 37 °C. Then, a volume of 9 mL deionized water was added. Prepared sample was placed in a 37 °C room. Every 1 h, a total of 100 μL solution was taken out to perform HPLC (Agilent Technologies, USA) analysis.

*In Vitro Antibacterial Activity*: A volume of 100 μL of PBS, BG, 20 μм **cyclo-zp80r** free drug, and the gel containing 20 μм **cyclo-zp80r** were added in four tubes, respectively. Tubes were placed at 37 °C until two gels were

solidified. *PA* 03 and *SA* 1114 cells were adjusted to CFU = $10^6$ per mL, respectively, and mixed them with the volume ratio of 1:1. Then, 900 µL of bi-microbial cultures were added to each tube and incubated at 37 °C. The CFUs were counted every 1 h.

*Ex Vivo Studies—Mechanical Pressure Test*: The pork skin was purchased from local market in Hong Kong. Before the experiment, pork skin was diced into smaller pieces and a hole was made by a punch. Hydrogel was stained by the crystal violet for a better visualization and then injected into the created wound at room temperature. Next, it was incubated at 37 °C to form rigid gel. Hydrogel-coating pork skin was subjected to the mechanical pressure of stretching, twisting, bending and compressing respectively.

*Antibacterial Activity on Human Skin*: Fresh human skin samples were ordered from Genoskin, France. According to French law L.1245 CSP, it is considered as "product and element of body taken during a surgical procedure", and used for scientific research only. The vendor Genoskin clarified in the lot release certificate that they were taken from the abdomen of a 45-year-old female during a surgical procedure. The epidermal wound was then fabricated. Next, *PA* 03 and *SA* 1114 cells were adjusted to $OD_{600}$ = 0.1, diluted tenfold in PBS, and mixed with the volume ratio of 1:1. Prepared bi-microbial cultures (10 µL) were added to the wound sites for four skin samples and one skin sample was treated with equivalent PBS as a non-infected control. After 30 min incubation, four infected skins were treated with PBS, F11 BG, 200 µM **cyclo-zp80r** solution, and the F11 hydrogel containing 200 µM **cyclo-zp80r** (10 µL for each group). At intervals (1, 3, and 6 h), a volume of 1 µL solution from the wound sites were sampled to count the bi-microbial colonies. Before sampling, human skin was temporarily placed at 4 °C until the gel returned to a fluid state, and the solution was pipetted up and down gently at least ten times for better homogenization.

*Histological Study*: Skin samples abovementioned were immersed in 4% paraformaldehyde (Sigma-Aldrich, USA) for 48 h. Then, they were embedded in liquid paraffin for sectioning and mounted in glass slides. After H&E staining, tissues were filmed by the microscopy.

*In Vivo Studies*: The mouse experiments were approved by animal ethics committee, the Chinese University of Hong Kong with the approval number of 23-215-HMF. Female BALB/c mice (18 – 20 g) were shaved to expose the back skin. Mice were randomly divided into four groups of six. A 4 cm × 4 cm wound was fabricated using a puncher on bare skin. Two days later, *PA* 03 and *SA* 1114 cells were adjusted to $10^6$ CFU $mL^{-1}$, respectively, mixed with the volume ratio of 1:1, and then a volume of 10 µL of the mixture were dropped onto the wound. After 1 h of infection, wounds were treated with equivalent volume of PBS, F11 hydrogel containing 200 µM **cyclo-zp80r** or a thin patch of FA cream. The wound without bacterial infection was set as the negative control. Wounds were treated in the same way for subsequent two days. On the third day, a volume of 10 µL PBS was dropped to each wound site. After homogenization, the solution was sampled to count the bi-microbial colonies. Wound healing condition was meanwhile monitored for 10 days.

*Statistical Analysis*: All experiments were triplicated unless specified. The results were expressed as mean ± standard error. Data analysis was performed by ANOVA and *t*-tests, where * represents $p < 0.05$, ** represents $p < 0.01$, *** represents $p < 0.001$, and **** represents $p < 0.0001$.

## Supporting Information

Supporting Information is available from the Wiley Online Library or from the author.

## Acknowledgements

The authors are thankful to Prof. Cuixia Chen for providing bacterial strain *SA* ATCC 25923. The authors are thankful to Dr. Xiaoqing Fan, Ms. Kangna Cao, and Ms. Baoqi Li for providing RBC for the hemolysis test. The authors acknowledge the financial support from the Research Grants Council of Hong Kong (Grant No. C5026-16G) and the Health and Medical Research Fund Hong Kong (Grant No. 21200782 and 23220102). Dr. KF Chan would like to dedicate this work to Professor Tak-Hang Chan on the occasion of his 83rd birthday.

## Conflict of Interest

The authors declare no conflict of interest.

## Data Availability Statement

The data that support the findings of this study are available from the corresponding author upon reasonable request.

## Keywords

bi-microbial infection, broad-spectrum antibacterial, cyclic peptide, human skin infection, mouse wound infection model, themosensitive hydrogel

Received: October 29, 2024
Published online: December 6, 2024

[1] S. Y. Wang, H. Kim, G. Kwak, H. Y. Yoon, S. D. Jo, J. E. Lee, D. Cho, I. C. Kwon, S. H. Kim, *Adv. Sci.* **2018**, *5*, 1800852.
[2] A. J. Alanis, *Arch. Med. Res.* **2005**, *36*, 697.
[3] J. H. Kwon, W. G. Powderly, *Science* **2021**, *373*, 471.
[4] J. N. Pendleton, S. P. Gorman, B. F. Gilmore, *Expert Rev. Anti Infect. Ther.* **2013**, *11*, 297.
[5] E. Akturk, L. D. R. Melo, H. Oliveira, A. Crabbe, T. Coenye, J. Azeredo, *Biofilm* **2023**, *6*, 100147.
[6] R. M. Epand, C. Walker, R. F. Epand, N. A. Magarvey, *Biochim. Biophys. Acta* **2016**, *1858*, 980.
[7] Q. Cheng, P. Zeng, *Curr. Pharm. Des.* **2022**, *28*, 3527.
[8] D. Juretic, J. Simunic, *Expert Opin. Drug Discov.* **2019**, *14*, 1053.
[9] L. Yi, P. Zeng, K.-Y. Wong, K.-F. Chan, S. Chen, *LWT* **2021**, *152*, 112412.
[10] S. Namjoshi, H. A. Benson, *Biopolymers* **2010**, *94*, 673.
[11] K. I. Wong, S. Wang, M. Li, G. Zhao, C. Wang, L. Wu, H. Fan, M. Yao, M. Lu, *Chem. Eng. J.* **2024**, *483*, 149287.
[12] H. Li, S. Duan, L. Li, G. Zhao, L. Wei, B. Zhang, Y. Ma, M. X. Wu, Y. Mao, M. Lu, *Adv. Mater.* **2024**, *36*, 2310532.
[13] X. Zhao, M. Zhang, I. Muhammad, Q. Cui, H. Zhang, Y. Jia, Q. Xu, L. Kong, H. Ma, *Antibiotics* **2021**, *10*, 1465.
[14] a) D. I. Andersson, D. Hughes, J. Z. Kubicek-Sutherland, *Drug Resist. Update* **2016**, *26*, 43; b) D. Cheng, R. Tian, T. Pan, Q. Yu, L. Wei, J. Liyin, Y. Dai, X. Wang, R. Tan, H. Qu, M. Lu, *Bioact. Mater.* **2024**, *35*, 517.
[15] a) E. M. C. Chung, S. N. Dean, C. N. Propst, B. M. Bishop, M. L. van Hoek, *NPJ Biofilms Microbiol.* **2017**, *3*, 9; b) P. W. Woods, Z. M. Haynes, E. G. Mina, C. N. H. Marques, *Front. Microbiol.* **2019**, *9*, 3291.
[16] Z. Lai, X. Yuan, H. Chen, Y. Zhu, N. Dong, A. Shan, *Biotechnol. Adv.* **2022**, *59*, 107962.
[17] R. Maharjan, A. I. Khan, M. Nadeem-Ul-Haque, M. Maresca, M. I. Choudhary, F. Shaheen, S. U. Simjee, *Probiotics Antimicrob Proteins* **2022**, *14*, 391.
[18] C. Xu, C. Liu, K. Chen, P. Zeng, E. W. C. Chan, S. Chen, *Commun. Biol.* **2022**, *5*, 613.
[19] F. A. Gogry, M. T. Siddiqui, I. Sultan, Q. M. R. Haq, *Front. Med.* **2021**, *8*, 677720.
[20] H. C. Flemming, J. Wingender, *Nat. Rev. Microbiol.* **2010**, *8*, 623.
[21] R. A. G. daSilva, I. Afonina, K. A. Kline, *Curr. Opin. Microbiol.* **2021**, *63*, 117.

[22] D. B. Kearns, *Nat. Rev. Microbiol.* **2010**, *8*, 634.
[23] S. Rutschlin, T. Bottcher, *Chem. Eur. J.* **2020**, *26*, 964.
[24] D. Ciumac, H. Gong, X. Hu, J. R. Lu, *J. Colloid Interface Sci.* **2019**, *537*, 163.
[25] N. Paracini, E. Schneck, A. Imberty, S. Micciulla, *Adv. Colloid Interface Sci.* **2022**, *301*, 102603.
[26] H. Strahl, L. W. Hamoen, *Proc. Natl. Acad. Sci. USA* **2010**, *107*, 12281.
[27] H. Li, X. Zhou, Y. Huang, B. Liao, L. Cheng, B. Ren, *Front. Microbiol.* **2020**, *11*, 622534.
[28] L. Radlinski, S. E. Rowe, L. B. Kartchner, R. Maile, B. A. Cairns, N. P. Vitko, C. J. Gode, A. M. Lachiewicz, M. C. Wolfgang, B. P. Conlon, *PLoS Biol.* **2017**, *15*, e2003981.
[29] D. H. Limoli, J. Yang, M. K. Khansaheb, B. Helfman, L. Peng, A. A. Stecenko, J. B. Goldberg, *Eur. J. Clin. Microbiol. Infect. Dis.* **2016**, *35*, 947.
[30] K. Zhao, L. Du, J. Lin, Y. Yuan, X. Wang, B. Yue, X. Wang, Y. Guo, Y. Chu, Y. Zhou, *Front. Microbiol.* **2018**, *9*, 2287.
[31] R. Serra, R. Grande, L. Butrico, A. Rossi, U. F. Settimio, B. Caroleo, B. Amato, L. Gallelli, S. de Franciscis, *Expert Rev. Anti Infect. Ther.* **2015**, *13*, 605.
[32] G. Lu, G. Zhao, S. Wang, H. Li, Q. Yu, Q. Sun, B. Wang, L. Wei, Z. Fu, Z. Zhao, L. Yang, L. Deng, X. Zheng, M. Cai, M. Lu, *Adv. Sci.* **2024**, *11*, e2306964.
[33] Y. Zhao, B. Yi, J. Hu, D. Zhang, G. Li, Y. Lu, Q. Zhou, *Adv. Funct. Mater.* **2023**, *33*, 2300710.
[34] J. L. Soriano-Ruiz, A. C. Calpena-Campmany, M. Silva-Abreu, L. Halbout-Bellowa, N. Bozal-de Febrer, M. J. Rodríguez-Lagunas, B. Clares-Naveros, *Int. J. Biol. Macromol.* **2020**, *142*, 412.
[35] J. Xiong, Z. R. Yang, N. Lv, K. Du, H. Suo, S. Du, J. Tao, H. Jiang, J. Zhu, *Macromol. Rapid Commun.* **2022**, *43*, e2200176.
[36] X. Peng, C. Ding, Y. Zhao, M. Hao, W. Liu, M. Yang, F. Xiao, Y. Zheng, *Front. Bioeng. Biotechnol.* **2022**, *10*, 831007.
[37] Y. Liang, J. He, B. Guo, *ACS Nano* **2021**, *15*, 12687.
[38] P. Zeng, Q. Cheng, J. Xu, Q. Xu, Y. Xu, W. Gao, K.-Y. Wong, K.-F. Chan, S. Chen, L. Yi, *Food Control* **2022**, *135*, 108827.
[39] A. Micsonai, E. Moussong, F. Wien, E. Boros, H. Vadaszi, N. Murvai, Y. H. Lee, T. Molnar, M. Refregiers, Y. Goto, A. Tantos, J. Kardos, *Nucleic Acids Res.* **2022**, *50*, W90.
[40] J. Rey, S. Murail, S. de Vries, P. Derreumaux, P. Tuffery, *Nucleic Acids Res.* **2023**, *51*, W432.